


Enhancing hydrogel toughness by uniform cross-linking using modified polyhedral oligomeric silsesquioxane

Sirawit Pruksawan¹, Jeremy Weixiong Reuben Lim¹, Yock Leng Lee ², Zehuang Lin², Heng Li Chee¹, Yi Ting Chong¹, Hong Chi ³✉ & FuKe Wang¹✉

The use of macro cross-linkers is one of the most effective approaches for developing tough hydrogels. However, the presence of uneven cross-linking and the resulting hydrogel inhomogeneity restrict further improvement. Here, we achieve uniform cross-linking by employing polyhedral oligomeric silsesquioxane (POSS)-grafted acrylated polyethylene glycol (PEG) as a cross-linker to enhance the toughness of hydrogels. The nano-sized hard silica core of POSS facilitates energy dissipation, and its dissolved form ensures uniform cross-linking through molecular-level dispersion. The peripheral acrylate groups introduce multiple interacting points, and the physical entanglements of long-chain PEG contribute to enhanced toughness. Incorporating acrylated POSS-PEG into polyacrylamide hydrogel yields enhanced properties such as toughness of up to 6531 kJ m^{-3} and break elongation up to 9455%, where the length of PEG chains grafted onto POSS is demonstrated to play a crucial role in facilitating energy dissipation and achieving high toughness.

¹Institute of Materials Research and Engineering (IMRE), Agency for Science, Technology, and Research (A*STAR), 2 Fusionopolis Way, Innovis #08-03, Singapore 138634, Republic of Singapore. ²College of Design and Engineering, National University of Singapore (NUS), 4 Engineering Drive 3, Singapore 117583, Republic of Singapore. ³Shandong Provincial Key Laboratory of Molecular Engineering, School of Chemistry and Chemical Engineering, Qilu University of Technology (Shandong Academy of Sciences), Jinan 250353, China. ✉email: chihong@qlu.edu.cn; wangf@imre.a-star.edu.sg

The successful practical applications of hydrogels in fields like tissue engineering and drug delivery have prompted an increasing shift towards the development of highly tough hydrogels for real-world utilization^{1–4}. Hydrogels generally exhibit poor mechanical properties compared to polymer resins due to their high-water content and inhomogeneity, and their mechanical performance is influenced by factors such as the structure of the polymer network, chemical composition, and cross-linking density⁵. Hence, numerous approaches have been developed to optimize these factors, with the cross-linking strategy being recognized as one of the most effective techniques for introducing energy dissipation and achieving high toughness in hydrogels^{6–10}.

Conventionally, molecular chemical cross-linkers have been employed in hydrogels to achieve mechanical stability and controlled swelling behavior¹¹. For example, in biomedical applications of polyacrylate hydrogels, molecular cross-linkers like diethylene glycol diacrylate (DEGDA), poly(ethylene glycol) diacrylate (PEGDA), and *N,N'*-methylenebis(acrylamide) (MBAA), tetraethyleneglycol dimethacrylate (TEGDMA) have been widely utilized^{12–14}. However, small molecule cross-linkers exhibit less physical entanglement within the polymer chains, resulting in weak hydrogels with limited mechanical properties. In recent years, macro cross-linkers, such as silica and graphene have gained popularity in the toughening of hydrogels due to their ability to be easily functionalized on the surface and covalently cross-linked into the polymer chains at the nano-/micrometer scale^{15,16}. The resulting hydrogels exhibit high extensibility and resilience as the stiff core of the cross-linker can enhance toughness through inducing microcracking or crack deflection while the surface-grafted polymer chains can help to distribute a significant portion of the applied energy through a dynamic cross-linking^{17,18}. The use of macro cross-linkers, on the other hand, can result in uneven cross-linking within the hydrogel network because of their large size. Macro cross-linkers induce dense cross-linking in their vicinity, while other regions may exhibit lower cross-linking density¹⁹. Additionally, high loading of macro cross-linkers leads to aggregation and a poor degree of dispersion, resulting in the non-uniform distribution of applied force within the hydrogel. As a consequence, this decreases the overall mechanical properties²⁰. Therefore, achieving uniform cross-linking throughout the entire hydrogel matrix with a macro cross-linker-like structure is crucial for maintaining consistent mechanical properties as well as swelling behavior.

In the present work, we aim to achieve uniform cross-linking by utilizing polyhedral oligomeric silsesquioxane (POSS), which is the smallest form of hybrid silica-based materials, to construct the smallest possible macro cross-linker core with grafted long-chain polymers. POSS is a unique class of hybrid materials with a well-defined nanostructure, three-dimensional (3D) configuration, and customizable organic groups at the periphery^{21,22}. Grafting multiple long-chain acrylated polyethylene glycols (PEG) onto POSS can result in a promising cross-linker that synergistically enhances the toughness of hydrogel networks through multiple mechanisms. First, the nano-sized hard and cage-like silica core facilitates energy dissipation by acting as a rigid and reinforcing component within the hydrogel. It helps to transfer stress within the hydrogel by effectively redirecting the stress from the softer regions of the hydrogel to the harder and more rigid silica core. The rigid nature of the silica core enables effective stress transfer and distribution, preventing localized failure in the hydrogel^{23–26}. In addition, the well-defined structure and ultra-small size of POSS also offer significant advantages, as it can dissolve in solution rather than disperse like nanoparticles²⁷. This characteristic ensures uniform dispersion of the POSS cross-linker at a molecular level. Furthermore, the acrylate groups at the end of the

PEG chain introduce multiple interacting points. Last, the physical entanglements of the long-chain PEGs further contribute to the enhanced properties. Our results showed that the incorporation of POSS-grafted acrylated polyethylene glycol (Ac-POSS-PEG) within polyacrylamide (PAM) hydrogels led to an exceptionally high toughness (up to 6531 kJ m⁻²), high elongation at break (up to 9455%), and high swelling capacity (up to 4425%), despite its high-water content of 60–70%. The molecular length of acrylated PEGs on POSS has been demonstrated to be crucial in enhancing gel formation and mechanical properties by increasing the number of physical entanglements and promoting the formation of a highly interpenetrating network within the hydrogel. Our research reveals the significant impact of the molecular length of the polymers grafted onto POSS on the mechanical properties of hydrogels, a finding not previously reported to our knowledge. Furthermore, this study highlights the potential of the ultra-small-sized, well-defined structure of POSS as a promising building block for grafting multiple reactive long-chain polymers, thereby facilitating the formation of a highly entangled and highly interpenetrating network, ultimately toughening the hydrogel.

Result and discussion

Design of Tough Hydrogels through Ac-POSS-PEG Cross-linker. We demonstrate the use of acrylated polyhedral oligomeric silsesquioxanes-polyethylene glycol (Ac-POSS-PEG) as a cross-linker to initiate a highly entangled and highly interpenetrating polymer network, enhancing the toughness of hydrogels. In the present work, acrylamide is used as a hydrogel monomer, while Ac-POSS-PEG functions as a cross-linker (Fig. 1a)²⁸. The hydrogel specimens were fabricated by a 3D printer with a resolution of up to 30 μm (Fig. 1b), and their resin composition is described in the Experimental Section. The use of Ac-POSS-PEG with a long PEG chain is expected to induce a highly interpenetrating polymer network with numerous physical entanglements and minimal chemical cross-links, as PEG's long molecular chains possess multiple interacting points through the increased number of available segments for interactions (Fig. 1c). The present approach maximizing physical entanglements while minimizing chemical cross-linkers holds great potential for improving the toughness of hydrogels, as it enables efficient dissipation of energy²⁹.

The photo-curing kinetics of PAM-Ac-POSS-PEG hydrogel precursors was evaluated by photo-differential scanning calorimetry (Photo-DSC) (Fig. 1d). After ultraviolet (UV) light irradiation, all photo-DSC curves show an exothermic peak corresponding to the photo-initiated radical polymerization of hydrogel precursors³⁰. Fig. 1d indicates that an increase in either the Ac-POSS-PEG content or the PEG molecular weight leads to a decrease in the reaction rate during the initial stage (0.00–0.02 min). This finding suggests that an increase in either the Ac-POSS-PEG content or the PEG molecular weight may potentially induce more physical gelation, which can impede the chemical cross-linking process and lead to a slower polymerization rate. The physical gelation induced by Ac-POSS-PEG hinders the mobility and accessibility of reactive sites on the polyacrylamide chains, causing the rate of chemical cross-linking to decrease. As a consequence, the efficient reaction between the polyacrylamide chains is affected, leading to a slower rate of covalent bond formation and, subsequently a slower overall polymerization rate during the initial stages of the reaction. In line with previous reports, the physical entanglement of polymer chains may potentially limit the accessibility of available reaction sites, suppressing the polymerization rate^{31,32}. Introducing longer poly(ethylene glycol) (PEG) chains in Ac-POSS-PEG results in a

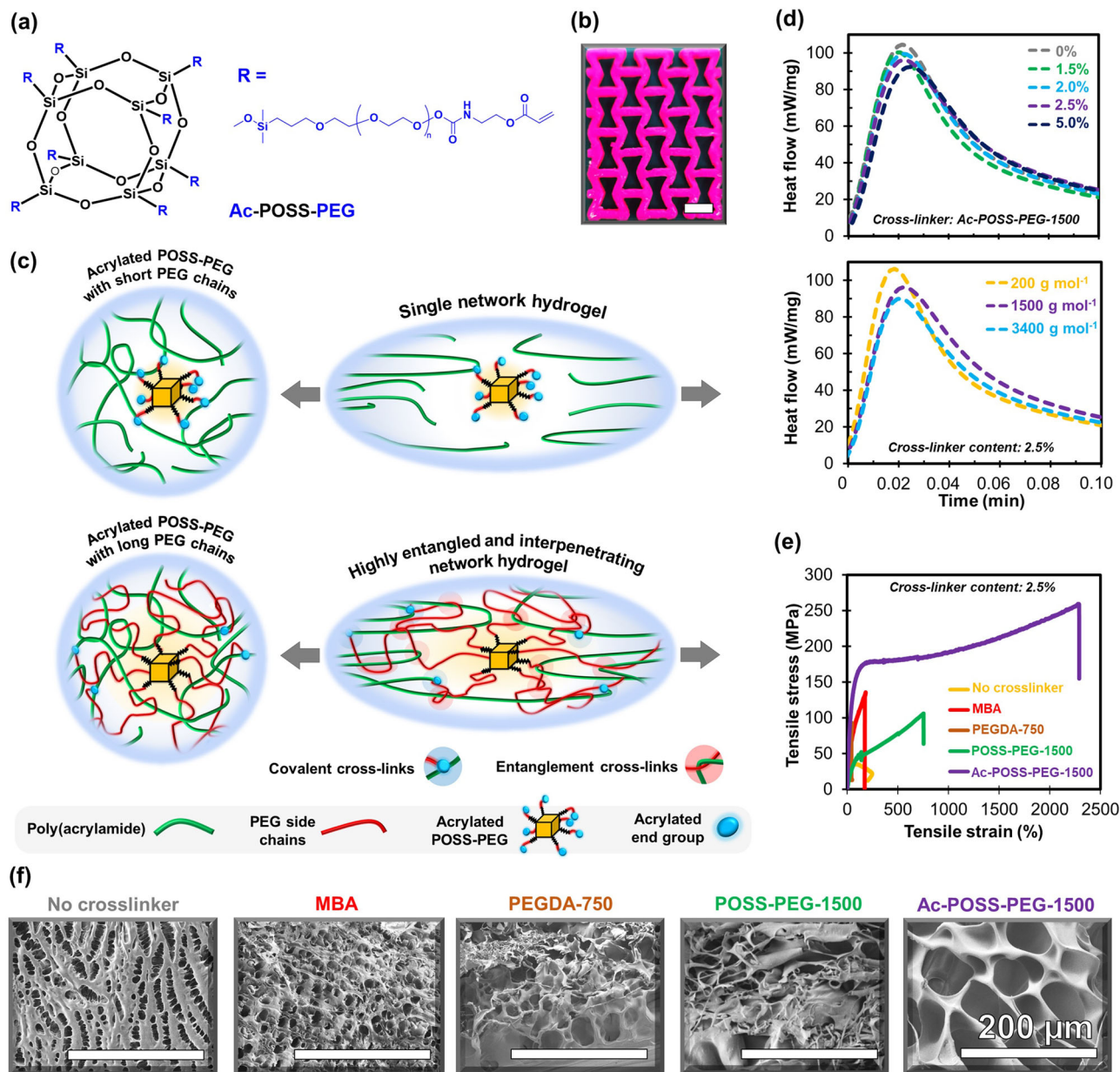


Fig. 1 Fabrication of polyacrylamide (PAM) hydrogels. **a** chemical structure of acrylate-terminated polyhedron oligomeric silsesquioxane-polyethylene glycol (Ac-POSS-PEG). **b** example of three dimensional (3D) printed specimens made from PAM-Ac-POSS-PEG hydrogels (Scale bar indicates 10 mm). rhodamine B was also added to this sample as a dye for the visualization of 3D-printed structures. **c** schematic representation of toughening mechanism by Ac-POSS-PEG. **d** photo-differential scanning calorimetry (DSC) profiles of the polymerization of uncured polyacrylamide (PAM) hydrogels with varying contents of Ac-POSS-PEG-1500 (top) and differing molecular weights of polyethylene glycol (PEG) (bottom). **e** and **f** a comparison of the tensile mechanical properties and morphology of PAM hydrogels prepared using different cross-linkers at a cross-linker content of 2.5% (Scale bar indicates 200 μm).

more pronounced decrease in the polymerization rate, possibly attributed to the significant formation of physical cross-links caused by the extended PEG chains.

To gain further insights into the cross-linking strategy effect on the mechanical performance of PAM hydrogels, different types of cross-linkers were employed, and their mechanical properties and microstructures are compared (Fig. 1e and f). In the absence of a cross-linker, the cross-sectional scanning electron microscope (SEM) image reveals a collapsed pore structure, typically occurring during the freeze-drying process. The neat PAM hydrogel, characterized by a loose network structure and low cross-link density, is unable to maintain its 3D network. Despite displaying an elongation of over 250%, the tensile strength of the

neat PAM hydrogel is lower than 35 kPa. A small molecular cross-linker, N,N'-methylenebisacrylamide (MBA), was used at a concentration of 2.5% (MBA-2.5%). The resulting hydrogel exhibits a porous structure with pore diameters ranging from 5 to 35 μm. As expected, the hydrogel network becomes brittle and significantly loses its flexibility^{29,33}. Consequently, the PAM-MBA-2.5% hydrogel demonstrates a brittle fracture behavior with a relatively high tensile strength of 183 kPa and a low fracture strain of 136%.

To further increase the length of the chemical cross-linker, we employed 2.5% polyethylene glycol diacrylate with a molecular weight of 750 g mol⁻¹ (PEGDA-750-2.5%) as polymeric cross-linker in the PAM hydrogel preparation, resulting in

inhomogeneous porous structures and extremely brittle fracture behavior. Similarly, employing unmodified octasilane POSS also led to a degradation of the mechanical properties of the PAM hydrogel due to its indissolubility. Additionally, we used hydroxyl-terminated POSS-PEG-1500 at a concentration of 2.5% (POSS-PEG-1500-2.5%) as a cross-linker model with only physical interaction. The results showed a significant improvement in both tensile strength and elongation at break. The hydrogel achieved values of up to 105 kPa for tensile strength and 746% for elongation at break. It is worth noting that hydroxyl-terminated POSS-PEG-1500 does not possess any photo-cross-linkable end groups. Therefore, its toughening effect primarily arises from the physical entanglements of POSS-PEG, highlighting its remarkable potential for enhancing the mechanical properties of hydrogels.

Surprisingly, PAM hydrogel cross-linked with acrylate-terminated POSS-PEG-1500 at a concentration of 2.5% (referred to as Ac-POSS-PEG-1500-2.5%) exhibits an exceptionally large pore size ranging from 46 to 120 μm . This pore size is relatively larger than that of typical chemical cross-linked PAM hydrogels previously reported^{34–36}. The PAM-Ac-POSS-PEG-1500-2.5% hydrogel, despite having a large porous structure, exhibits remarkable mechanical properties, with a tensile strength of 304 kPa, an elongation at break of 2,287%, and a tensile modulus of 520 MPa. The superior mechanical properties observed in PAM hydrogel using Ac-POSS-PEG as a cross-linker, compared to PAM hydrogel using other previously discussed cross-linkers, suggest a unique advantage of modified POSS as a hydrogel cross-linker. This enhanced mechanical performance is attributed to the benefits from small molecules of POSS core, as well as the macro cross-linking by acrylate PEG side chains. The small size of the POSS core enables its high dissolution in solution for uniform dispersion at a molecular level, while the acrylate PEG side chains on POSS contribute to physical entanglements and covalent cross-linking within the hydrogel. As a result, the toughness of the hydrogel is enhanced. Notably, when utilizing unmodified octasilane POSS alone or PEGDA alone, there is no significant enhancement observed in the mechanical properties of hydrogels, in contrast to the combination of POSS with acrylate PEG side chains. Significantly, the small size and presence of PEG chains on the periphery of the POSS molecule enable good solubility in aqueous solutions (Supplementary Fig. 1). This characteristic ensures uniform cross-linking of the hydrogel, which is crucial for achieving high-performance hydrogels.

Morphology and Swelling Behavior of PAM-Ac-POSS-PEG Hydrogels. To elucidate the morphological characteristics of PAM-Ac-POSS-PEG hydrogels, cross-sectional SEM images of PAM hydrogel cross-linked with different content and molecular weight of Ac-POSS-PEG are displayed in Fig. 2a. Hydrogels with a higher content of Ac-POSS-PEG exhibited increased visual opacity and generally displayed larger pore sizes with thicker pore walls. The formation of these larger porous structures can be attributed to the higher loading of Ac-POSS-PEG, which promotes a denser structure through increased cross-linking. However, when the Ac-POSS-PEG content exceeded certain thresholds (10%, 7.5%, and 1% for Ac-POSS-PEG with PEG molecular weights of 200, 1500, and 3400 g mol^{-1} , respectively), we observed non-interconnected porous structures with low porosity. This outcome is a result of the limited water solubility of Ac-POSS-PEG in the hydrogel precursor solution. Excessive loading induced aggregation of the Ac-POSS-PEG and leading to inhomogeneous cross-linking. It is important to note that insufficient loading of Ac-POSS-PEG may not enough to form stable 3D gel structures. For instance, hydrogels made with a low

content of Ac-POSS-PEG, like PAM-Ac-POSS-PEG-200-0.5%, PAM-Ac-POSS-PEG-200-1.5%, and PAM-Ac-POSS-PEG-1500-0.5%, do not form stable hydrogel structures and can be dissolved in water. On the contrary, the threshold can be decrease with the increase of the size of the PEG polymer chain. A significantly lower loading of Ac-POSS-PEG with large PEG molecular weight can lead to a greater degree of physical entanglement of polymer chains, which in turn promotes a higher degree of cross-linking and enhances the gel formation. Supplementary Fig. 2 shows the gel fraction as a function of Ac-POSS-PEG content with different PEG molecular weights. Interestingly, higher PEG molecular weights require significantly lower crosslinker concentrations to achieve gel fraction. The critical gelation concentrations for Ac-POSS-PEG with PEG molecular weights of 200, 1500, and 3400 g mol^{-1} were found to be 2.5%, 1.0%, and 0.5%, respectively. The results suggest that longer PEG molecular lengths lead to more physical entanglements, due to the increased number of available segments for interactions with other molecules, facilitating the easier formation of a stable gel. Furthermore, Supplementary Fig. 3 illustrates that at a fixed cross-linker concentration of 2.5%, increasing the PEG molecular weight on POSS leads to a higher glass transition temperature (T_g) of the hydrogel, implying the presence of physical entanglements that restrict the movement of polymer chains and contribute to the observed T_g increase³⁷. At an optimum concentration of Ac-POSS-PEG, the SEM images of PAM-Ac-POSS-PEG hydrogels show a very uniform porous morphology, which is likely due to the well-dissolved POSS cross-linker. This structure may facilitate the formation of a more interconnected network with better packing and distribution within the hydrogel matrix, resulting in a hydrogel with a consistent and organized porosity.

Fig. 2b illustrates the swelling ratio of various PAM hydrogels in deionized water at room temperature. It is noteworthy that the PAM hydrogel without any cross-linker lacks a gel fraction. Incorporating Ac-POSS-PEG-1500 at more than 1.5% successfully prevented hydrogel networks from dissolution and destruction, as observed in Fig. 2c. This result confirms the improved stability of hydrogel networks by POSS-PEG-1500. The PAM-Ac-POSS-PEG-1500-1.5% hydrogel displays the highest swelling ratio of 4,349% due to its relatively loose structure as shown in Fig. 2a. As expected, when the content of Ac-POSS-PEG-1500 increases, the swelling ratio of PAM hydrogels gradually decreases. This is attributed to the higher Ac-POSS-PEG-1500 content, which enhances cross-linking density, causing a denser network structure and stiffer mechanical properties. In addition, the molecular weight of PEG in Ac-POSS-PEG is another critical factor that significantly impacts the swelling behavior of hydrogels. From Fig. 2d, it can be observed that an increase in the molecular weight of PEG results in a substantial reduction in the swelling ratio of hydrogels. This can be attributed to the formation of a more interpenetrating polymer network due to an increase in physical entanglements and hydrogen bond interactions between polymer chains. It is worth noting that the figure does not include the swelling ratio of hydrogels that completely dissolved after being soaked in water for 18 h. The minimum cross-linker content required to achieve a gel fraction is 2.5%, 1.5%, and 0.5% for Ac-POSS-PEG-200, Ac-POSS-PEG-1500, and Ac-POSS-PEG-3400, respectively.

Mechanical Properties of PAM-Ac-POSS-PEG Hydrogels. The tensile mechanical properties of various PAM-Ac-POSS-PEG hydrogels are displayed in Fig. 3. From Fig. 3a, it can be seen that the PAM-Ac-POSS-PEG-1500-0.5% hydrogel exhibits a weak mechanical performance similar to neat PAM hydrogel, consistent with the fact that the PAM-Ac-POSS-PEG-1500-0.5%

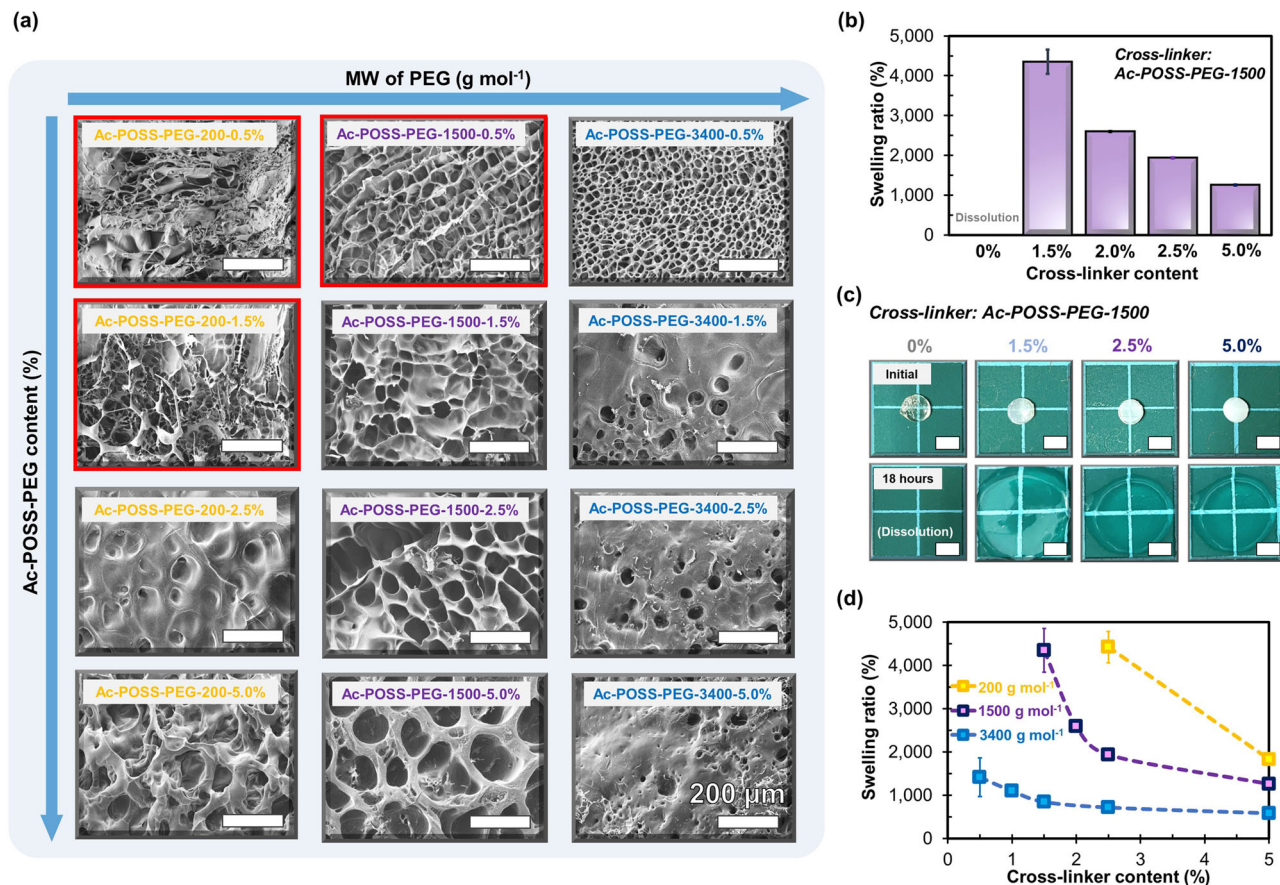


Fig. 2 Morphology and swelling behavior of polyacrylamide (PAM) hydrogels. **a** morphology of freeze-dried PAM-Ac-POSS-PEG hydrogels with varying the contents of acrylate-terminated polyhedral oligomeric silsesquioxane-polyethylene glycol with molecular weight of 1500 g mol⁻¹ (Ac-POSS-PEG-1500) and the molecular weights of polyethylene glycol (PEG) (Scale bar indicates 200 μm). The red borders in the image correspond to hydrogels that possess a low gel fraction of less than 90%. **b** equilibrium swelling ratio of PAM-Ac-POSS-PEG hydrogels with different contents of Ac-POSS-PEG-1500 **c** digital images of freeze-dried (initial) and swollen (18 h) PAM-Ac-POSS-PEG hydrogels with different content of Ac-POSS-PEG-1500 (Scale bar indicates 10 mm). **d** comparison of equilibrium swelling ratio of PAM-Ac-POSS-PEG hydrogels with varying contents of Ac-POSS-PEG and different molecular weights of PEG.

hydrogel dissolved entirely in deionized water after a day. Compared to neat PAM hydrogel, the PAM-Ac-POSS-PEG-1500-1% and PAM-Ac-POSS-PEG-1500-2% hydrogels do not show a large improvement in tensile strength but display an outstandingly high elongation at break of about 3,000%. Because of the existence of loose entanglements between polymer chains induced by the long PEG chains of Ac-POSS-PEG-1500, a significant enhancement of elongation at the break of PAM hydrogels can be achieved. For the PAM-Ac-POSS-PEG-1500-2.5% and PAM-Ac-POSS-PEG-1500-5% hydrogels, as more physical entanglements and chemical cross-links are introduced into the network, a more interpenetrating polymer network with a higher cross-linking density is obtained, resulting in more than a 50-fold toughness increase over the neat PAM hydrogel (Fig. 3b). When immersion in deionized water, the mechanical properties of all hydrogels were found to be significantly reduced. This is evident from Supplementary Fig. 4, which displays the tensile stress-strain curves of PAM-Ac-POSS-PEG hydrogels following a 4-hour immersion in deionized water, as compared to the original stress-strain curves shown in Fig. 3a. The volumetric expansion of the hydrogel during soaking leads to structural changes within the hydrogel network, including polymer chain separation and disruption of crosslinking^{38,39}. As a result, there is a notable decrease in both tensile strength and elongation.

Fig. 3c, d reveals the effect of Ac-POSS-PEG content at different PEG molecular lengths. It was found that for all PEG

molecular weights, the tensile strength increases with increasing the content of Ac-POSS-PEG, due to an increase in cross-link density (Fig. 3d: left). When the PEG molecular weight is higher, the tensile strength starts increasing at lower loading of Ac-POSS-PEG contents, due to the larger amount of physical cross-linking existing in hydrogels. On the other hand, the elongation at break initially increases with increasing Ac-POSS-PEG content until a stable gelation is achieved and then gradually decreases due to a denser cross-link network (Fig. 3d: centre). The maximum elongation at break for Ac-POSS-PEG with PEG molecular weight of 200, 1500, and 3400 g mol⁻¹ was determined to be 2.5, 1.0, and 0.5%, respectively, which corresponds to their critical gelation concentration (Supplementary Fig. 2). Besides, a more pronounced toughening effect is observed when using a larger PEG molecular length because more interpenetrating polymer network with more physical entanglements and hydrogen bond interactions are induced (Fig. 3d: right). At a very low cross-linker content of 0.5%, the high toughness of 5724 kJ m⁻³ was observed when a PEG molecular weight of 3400 g mol⁻¹ is used, attributing to the abundant physical entanglements and optimal chemical cross-links induced by the long PEG side chains, enabling the energy dissipation and thus toughening the hydrogels (Fig. 3c). The mechanical properties for the higher Ac-POSS-PEG-200 content are shown in Supplementary Fig. 5. Although there have been a limited number of studies incorporating multiple functionalized POSS molecules into hydrogels⁴⁰⁻⁴⁴, to the best

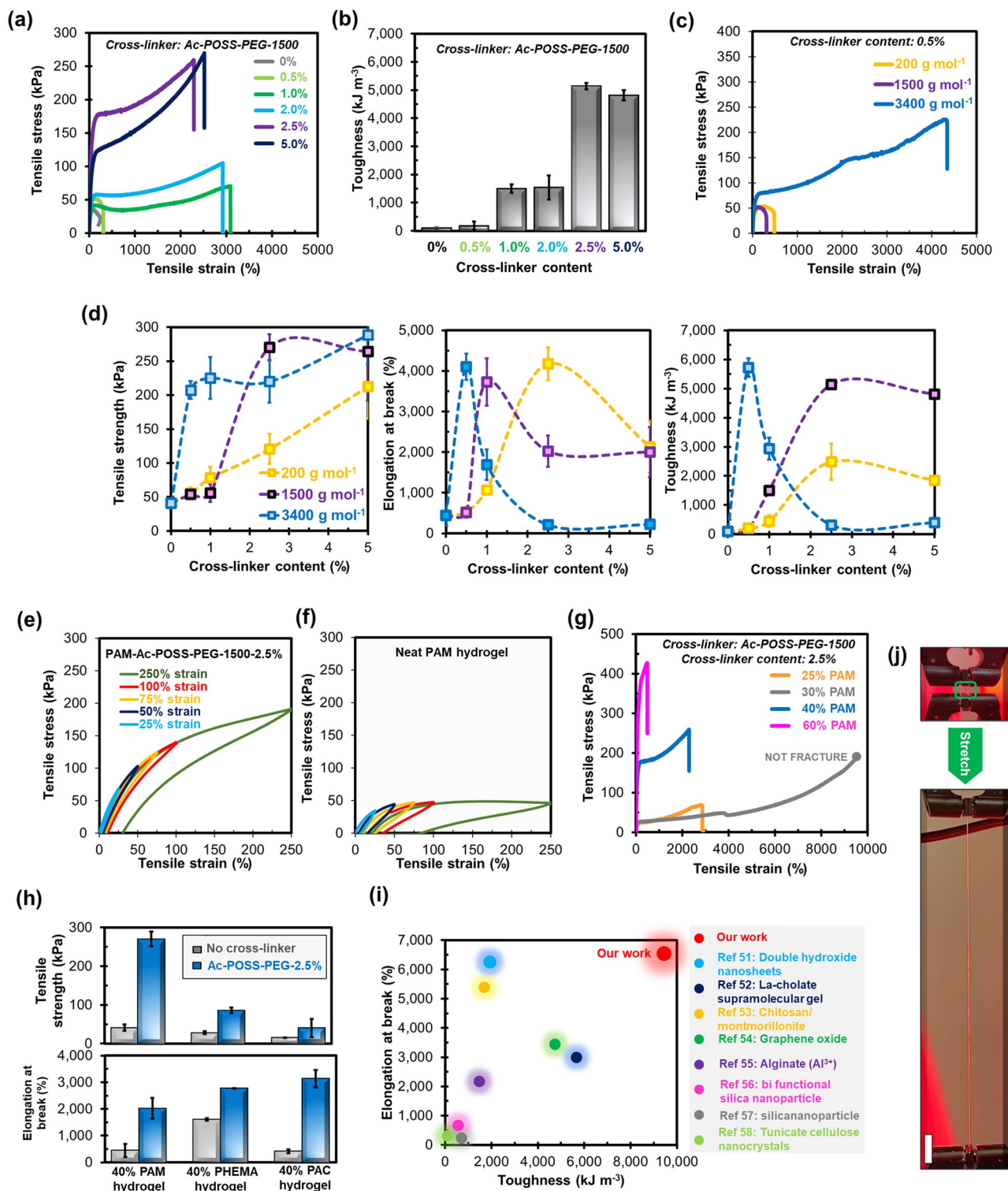


Fig. 3 Mechanical properties of polyacrylamide (PAM) hydrogels. **a** and **c** tensile stress-strain curves of PAM-Ac-POSS-PEG hydrogels with different contents of acrylate-terminated polyhedral oligomeric silsesquioxane-polyethylene glycol with molecular weight of 1500 g mol^{-1} (Ac-POSS-PEG-1500) and with different molecular weights of polyethylene glycol (PEG). **b** toughness of PAM-Ac-POSS-PEG hydrogels with different contents of Ac-POSS-PEG-1500. **d** tensile strengths, elongation at break and toughness of PAM-Ac-POSS-PEG hydrogels plotted as a function of cross-linker content and molecular weight of PEG. **e** and **f** representative hysteresis loops of neat polyacrylamide (PAM) and PAM-Ac-POSS-PEG-1500-2.5% hydrogels at varying maximum tensile strains, ranging from 25% to 250%. The dissipation energies corresponding to different maximum tensile strain levels are presented in Supplementary Fig. 7. **g** tensile stress-strain curves of PAM-Ac-POSS-PEG-1500-2.5% hydrogels with different acrylamide concentrations. **h** tensile strength and elongation at break of PAM, poly(2-hydroxyethyl methacrylate) (PHEMA) and poly(acrylic acid) (PAC) hydrogels prepared using Ac-POSS-PEG-1500 at 2.5%. **i** comparison of toughness and elongation at break of 30% PAM-Ac-POSS-PEG-1500 hydrogels developed in this work with various previously reported tough PAM hydrogels. **j** digital images of 30% PAM-Ac-POSS-PEG-2.5% hydrogel before and after stretching (Scale bar indicates 5 cm).

of my knowledge, this is the first successful design of a POSS cross-linker that effectively harnesses its unique structure and integrates the advantages of both small molecular and macro cross-linkers. We also elucidate the significant impact of the molecular length of the grafted polymers on POSS on the mechanical properties of hydrogels and thus achieve significant improvements in their toughness. Additionally, the PEG chains on POSS can participate in hydrogen bonding interactions with the amide groups in polyacrylamide through their hydroxyl groups, which may result in improved intermolecular interactions. Fourier transform infrared absorption (FT-IR) results suggest the presence of hydrogen bonding within PAM-POSS-PEG-1500 hydrogels (Supplementary Fig. 6). The neat PAM hydrogel displays a characteristic peak at 1130 cm^{-1} , corresponding to the C-N stretching of amides in the acrylamide chain^{45,46}. However, this peak diminishes upon the addition of the POSS-PEG-1500 cross-linker. Furthermore, in the PAM-POSS-PEG-1500-2.5% and PAM-POSS-PEG-1500-2.5% hydrogels, a new peak is observed around $1080\text{--}1093\text{ cm}^{-1}$, while this peak is absent in both POSS-PEG-1500 cross-linker and neat PAM hydrogel. This observation suggests the formation of interactions between polyacrylamide and the POSS-PEG crosslinker, such as hydrogen bonding. This interaction is likely the result of the hydroxyl groups of POSS-PEG forming bonds with the amide groups of polyacrylamides. Consequently, these interactions enhance the physical entanglements in the hydrogel due to the formation of additional bonds between the polymer chains.

Furthermore, tensile cyclic loading-unloading tests were conducted on the PAM-Ac-POSS-PEG-1500-2.5% hydrogel at various strain levels (Fig. 3e). At low tensile strains below 100%, the hysteresis loop was relatively small, indicating a higher degree of elastic behavior. Additionally, an overlap region was observed in adjacent stress-strain curves, indicating the self-recovery ability of the hydrogel. This suggests that the hydrogel can regain some of its original shape and mechanical properties. However, as the tensile strain increased to 250% and beyond, the hysteresis loop notably expanded, indicating substantially higher energy dissipation, as demonstrated in Supplementary Fig. 7. This suggests reduced stretching reversibility at such strain levels. The increase in the hysteresis loop size suggests the occurrence of irreversible deformation processes, such as plastic deformation or changes in the hydrogel network structure. A similar hysteresis behavior was observed in the neat PAM hydrogel, but it exhibited a lower tensile stress (Fig. 3f), which is in line with the tensile test results.

The mechanical properties of PAM hydrogels with varying concentrations of acrylamide and different hydrogel matrices are shown in Fig. 3g, h. Among all hydrogels investigated in this study, the largest elongation at break and toughness of more than 9,455% and $6,531\text{ kJ m}^{-3}$ were found in 30%-PAM-Ac-POSS-PEG-1500-2.5% hydrogel, which is attributed to the optimal balance between physical and chemical cross-links by entanglements and covalent bonds, respectively. The 30%-PAM-Ac-POSS-PEG-1500-2.5% hydrogel did not break even when applied with the maximum strain of the tensile testing machine (Fig. 3j). At a low acrylamide concentration of 25%, the 25%-PAM-Ac-POSS-PEG-1500-2.5% hydrogel has relatively weak fracture behavior possibly owing to its loose cross-linked network. The acrylamide concentration of higher than 30% leads to a reduced elongation at break and increased tensile strength as a denser cross-linked network is expected. In Fig. 3i, a comparison of the toughness and elongation at break is shown between various high-performance PAM hydrogels previously reported with the results in the present study. Our PAM-Ac-POSS-PEG hydrogel demonstrates outstanding mechanical properties that are comparable to those of double network hydrogels⁴⁷, slide-ring hydrogels⁴⁸, and other nanocomposite hydrogels⁴⁹ that are

currently regarded as the toughest hydrogel systems. Representative PAM-based hydrogels with high toughness include PAM-layered double hydroxide nanosheets⁵⁰, PAM-La-choleate supra-molecular gel⁵¹, PAM-chitosan/montmorillonite⁵², PAM-graphene oxide⁵³, PAM-alginate (Al^{3+})⁵⁴, PAM-bi functional silica nanoparticle⁵⁵, PAM-silicananoparticle⁵⁶ and PAM-tunicate cellulose nanocrystals⁵⁷. Particularly, the toughness and elongation at break of PAM-Ac-POSS-PEG hydrogels in the present study is exceptionally higher than most of the reported tough PAM hydrogels.

To further understand the toughening effect of hydrogels by Ac-POSS-PEG, the Ac-POSS-PEG is used for poly(2-hydroxyethyl methacrylate) (PHEMA) and poly(acrylic acid) (PAC) hydrogel matrices (Fig. 3h). By incorporating of Ac-POSS-PEG, the mechanical properties of all hydrogel matrices can be enhanced with different extent, most likely depending on the interaction between PEG chains of Ac-POSS-PEG and a monomer. More interacting points through the increased number of available segments for interactions with other molecules would induce more physical entanglements of polymer chains, promoting a higher interpenetrating polymer network and toughening effect. The results suggest that our proposed toughening approach by using POSS as a building block for grafting multiple long chain polymers can be applied to various hydrogel systems and thus should open up new design opportunities to produce ultra-tough hydrogels. The tough hydrogels developed in this study hold great promise in various biomedical engineering applications, particularly in tissue engineering^{58–60}. The exceptional toughness and significant elongation at break exhibited by these hydrogels enable them to closely mimic the mechanical properties of natural tissue. This unique characteristic empowers the hydrogel to offer vital mechanical support to cells and facilitates the promotion of tissue regeneration. Furthermore, the 3D printability of these hydrogels provides the capability to fabricate complex structures and patient-specific implants.

Conclusion

Inspired by the unique size and well-defined cage-like structure of polyhedral oligomeric silsesquioxane, we propose a general strategy for toughening hydrogels using POSS-grafted acrylated polyethylene glycol (Ac-POSS-PEG) as a cross-linker. The incorporation of Ac-POSS-PEG into the polyacrylamide (PAM) hydrogel matrix demonstrates the formation of a highly interpenetrating polymer network with numerous physical entanglements, optimal chemical cross-linking, and a uniform microstructure. The proposed cross-linker, Ac-POSS-PEG, integrates the advantages of both small molecular cross-linkers and macro cross-linkers, while also ensuring uniform cross-linking through its dissolution ability. Our results further indicate that the long acrylated PEG chains on POSS provide multiple points of interaction, thereby improving the ability to entangle polymer chains and enhancing energy dissipation capacity and toughening effects. At the optimal balance between physical and chemical cross-links, an ultra-tough hydrogel can be achieved with more than a 50-fold toughness increase over the neat PAM hydrogel. The molecular length of PEG grafted chains on POSS was found to have a considerable impact on the toughening effect, which suggests that the toughening mechanism is attributed to the substantial energy dissipation due to physical entanglements of the long PEG chains. Our study demonstrated that grafting long-chain polymers onto the small and defined POSS forms a highly interpenetrating network structure with multiple physical entanglements, resulting in a remarkable increase in toughness that far surpasses what can be achieved with long-chain polymers alone.

Table 1 Material composition of various polyacrylamide (PAM) hydrogel precursors.

Sample name	Cross-linker	Resin compositions Acrylamide: H ₂ O	Additive	
			Cross-linker (weight %)	LAP (weight %)
Neat PAM	–	40:60	–	0.5
PAM-MBA-2.5%	MBA		2.5	
PAM-POSS-2.5%	POSS			
PAM-PEGDA-750-2.5%	PEGDA-750			
PAM-POSS-PEG-1500-2.5%	POSS-PEG-1500			
PAM-Ac-POSS-PEG-200-2.5%	Ac-POSS-PEG-200			
PAM-Ac-POSS-PEG-1500-2.5%	Ac-POSS-PEG-1500			
PAM-Ac-POSS-PEG-3400-2.5%	Ac-POSS-PEG-3400			
PAM-Ac-POSS-PEG-1500-0.5%	Ac-POSS-PEG-1500	40:60	0.5	0.5
PAM-Ac-POSS-PEG-1500-1.5%			1.0	
PAM-Ac-POSS-PEG-1500-1.5%			1.5	
PAM-Ac-POSS-PEG-1500-2.0%			2.0	
PAM-Ac-POSS-PEG-1500-5.0%			5.0	
25% PAM-Ac-POSS-PEG-1500-2.5%	Ac-POSS-PEG-1500	25:75	0.5	0.5
30% PAM-Ac-POSS-PEG-1500-2.5%		30:70		
60% PAM-Ac-POSS-PEG-1500-2.5%		60:40		

The percentages are based on mass percentage.

Experimental Section

Materials. Acrylamide (AM) ($\geq 99\%$ purity), 2-hydroxyethyl methacrylate (HEMA) (97% purity), and acrylic acid (99% purity) from Sigma-Aldrich (Singapore) were selected as hydrogel monomers and used as received. A traditional cross-linking agent, N,N'-methylenebisacrylamide (MBA) was obtained from Sigma-Aldrich (Singapore). SH1310 octasilane POSS was purchased from Hybrid Plastics Inc (USA). Allyl bromide was obtained from Sigma-Aldrich (Singapore) and distilled and stored under 4 Å molecular sieves. Platinum (0)-1,3-divinyl-Allyl,1,1,3,3-tetramethyldisiloxane (Karstedt's catalyst) and dibutyltin dilaurate (DBTDL) were obtained from Sigma-Aldrich (Singapore) and used as received. 2-isocyanatoethyl acrylate was purchased from TCI chemicals and used as received. Polyethylene glycol (PEG) with a molecular weight of about 200 g mol^{-1} (PEG-200, TCI Chemical, Japan), 1500 g mol^{-1} (PEG-1500, Sigma-Aldrich, Singapore), and 3400 g mol^{-1} (PEG-3400, Aldrich Chemical Company Inc., Singapore) was used as precursors for the synthesis of acrylate-terminated POSS-PEG (Ac-POSS-PEG). Sodium hydroxide (NaOH), tetrahydrofuran (THF), dichloromethane, magnesium sulfate (MgSO_4), and anhydrous toluene were obtained from Sigma-Aldrich (Singapore). Lithium phenyl-2,4,6-trimethylbenzoylphosphine oxide (LAP) photoinitiator was received from TCI Chemical (Singapore). Polyethylene glycol diacrylate (PEGDA) with a molecular weight of 750 g mol^{-1} was obtained from Sigma-Aldrich (Singapore).

Synthesis of the acrylate-terminated POSS-polyethylene glycol (Ac-POSS-PEG). The synthesis of the Ac-POSS-PEG was performed under standard Schlenk conditions (Supplementary Fig. 8). First, PEG (20 mmol), NaOH (0.32 g, 8 mmol) was added to 200 mL THF in a two-neck round-bottom flask (RBF) under an argon atmosphere with a condenser attached. The suspension was stirred and brought to 50°C . Allyl bromide (2.90 g) was added dropwise to the mixture and was refluxed for 12 h. The suspension was then cooled and filtered. The volatiles were evaporated, and the residue was redissolved in dichloromethane and washed with deionized water, brine, and dried over MgSO_4 . The suspension was then filtered, and the volatiles were removed under reduced pressure to obtain a light-yellow oil ($>80\%$ yield), denoted as Compound-1.

Second, the synthesis of POSS-PEG (Compound-2) was performed using a modified procedure described previously^{61,62}.

In a flamed dried two-neck RBF under an argon atmosphere, 8 eq. of Compound-1 was added and dissolved in anhydrous toluene. Subsequently, 1 eq. of octasilane POSS was added to the solution. 1 weight % of Karstedt's catalyst was added to the mixture and stirred under inert conditions at 80°C for 24 h. The reaction was then cooled to room temperature and filtered through a celite. The volatiles were removed under reduced pressure to obtain the product. The completion of the reaction was monitored using proton nuclear magnetic resonance (^1H NMR, JEOL ECA500II spectrometer) by the disappearance of allyl bonds at 4.9–5.1 ppm (Supplementary Fig. 9).

Ac-POSS-PEG (Compound-3) was synthesized via the condensation process of an isocyanate and alcohol. In a two-neck flame-dried RBF under inert conditions, 1 eq. of POSS-PEG and 8.2 eq. of 2-isocyanatoethyl acrylate were added. Toluene was added to make a 40 weight % solution. 1 weight % of DBTDL was then added, and the solution was stirred for 48 h at room temperature. The volatiles were removed under reduced pressure to obtain Ac-POSS-PEG.

Preparation and 3D printing of hydrogels. Polyacrylamide (PAM) hydrogel precursor was prepared as follows: A specified amount of cross-linker was dissolved in deionized water by ultrasonic treatment first. Subsequently, acrylamide monomer and LAP were added to the dispersion and sonicated for a few minutes to disperse the components evenly. The hydrogel compositions and the corresponding samples' names are shown in Table 1. It should be noted that all percentages mentioned in this paper are mass percentages. Additionally, all PAM hydrogels in this paper have an Acrylamide:H₂O ratio of 40:60, unless otherwise specified.

Hydrogel precursors were 3D printed on an Anycubic Photon M3 printer (Shenzhen Anycubic Technology Co., Ltd., China). The printer uses a liquid crystal display (LCD) shadow masking technique to form 3D prints and can achieve a printing accuracy of $4,096 \times 2,560$ pixels (4K). The wavelength of the projected ultraviolet light emitting diodes (UV-LED) light by the printer is 405 nm. All specimens were 3D printed in a rectangular shape of width 100 mm, height 35 mm, and thickness 1.6 mm. The rectangular-shaped model was saved in STL (Stereolithography) format and was imported into the Anycubic Photon Workshop 3D Slicer software in order to create the slicing file. The thickness

of each printing layer was set to 0.05 mm and the light intensity was set to 70%. The exposure time of the first 3 layers was 15 seconds, and the exposure time of each layer was 7.5 seconds. After importing the slicing file, the prepared hydrogel precursor was poured into the printer's vat, and the printing proceeded layer by layer. Subsequently, the printed specimens were post-cured in a UV oven before further testing or characterization.

Characterization of hydrogels. Photo-differential scanning calorimetry (Photo-DSC) was used to investigate the cure kinetics of a photo-initiated polymerization of acrylamide monomers mixed with different cross-linkers. A Q100 apparatus (TA instruments, Japan) equipped with a photo calorimeter accessory (Novacure 2100, EXFO Photonic Solutions Inc.) was used under a nitrogen flow at 50 ml min⁻¹. The hydrogel precursor was placed in a hermetic pan using a microsyringe with a sample size of about 4 mg. An empty hermetic pan was used as reference material. The DSC curves were generated after the UV light was turned on.

Field-emission scanning electron microscope (SEM) was used for morphological studies. A JEOL JSM6700F electron microscope (Japan) was operated at 5 kV. The hydrogel specimens were cut into rectangles of 1 cm × 1 cm × 1 cm, soaked in deionized water for 30 min, and freeze-dried overnight using a Martin Christ freeze dryer (Germany). The specimens were then mounted on an aluminum stub and sputter coated with gold in a sputter coater (JEOL JFC-1600 auto fine coater, Japan) for 25 seconds using JEOL JFC-1600 auto fine coater (Japan). The ImageJ software was utilized to determine the average pore size, pore distribution, and porous structure of the hydrogels.

Swelling test of hydrogels was carried out in deionized water at room temperature. The hydrogel specimens were cut into a circular disc of about 1 cm in diameter and freeze-dried overnight. After initial weighing, the specimens were soaked in deionized water for a day. To determine the percent weight change, the specimens were weighed periodically after removing them from the deionized water and wiping off moisture on their surface. The swelling ratio of hydrogels is calculated as the percentage increase in weight after the hydrogel has been immersed in water and allowed to swell. This measurement represents the extent to which the hydrogel can absorb and retain water during swelling.

The gel fraction of hydrogels was calculated based on the ratio between the dried weight (W_d) and extracted dried gel weight (W_e)⁶³, representing the proportion of the hydrogel that remained after the removal of unreacted or soluble components. The W_d was measured after drying the hydrogel in a 45 °C oven for one day. Then, the dried hydrogels were soaked against deionized water for one day at 37 °C to remove the soluble fraction and dried in a 45 °C oven for one day prior to measuring W_e .

Differential scanning calorimetry (DSC) was conducted using a Q100 apparatus (TA Instruments) with a nitrogen flow rate of 50 ml min⁻¹. Approximately 5 mg of freeze-dried hydrogel specimens was sealed in a hermetic pan and an empty hermetic pan was used as reference material. The specimens were heated repeatedly between 25 and 180 °C at 20 °C min⁻¹ and their glass transition temperatures (T_g s) were measured at the second heating scan.

Tensile test of hydrogels was carried out by an Instron 5569 double-column universal testing machine (Instron Corporation, United States) with a 100-N load cell. The nominal strain was obtained by normalizing the displacement with the initial gauge length of the specimen. As-prepared hydrogel specimens were cut into a strip of 10 mm × 60 mm × 1.6 mm and fixed with

pneumatic grips. The specimens were extended at a strain rate of 40 mm minute⁻¹ until it fractures. The extensometer was removed after the yield point can be determined. Once the extensometer was removed, the strain control was switched from extensometer to displacement rate. To ensure reproducibility, a minimum of 3 samples were tested under each condition, and the data was averaged. The tensile strength of hydrogels was determined by dividing the maximum load by the original cross-sectional area of the test specimen. The tensile modulus of hydrogels was determined from the linear region of the measured tensile stress-strain curves. The toughness was determined as the area under the tensile stress-strain curve, representing the energy absorbed by the material before fracture or failure. The presented tensile stress-strain curves in the figures are representative examples selected from the measurements conducted on multiple specimens. For the hysteresis tests, the hydrogel specimens were subjected to repeated cycles of tensile loading and unloading at a strain rate of 40 mm minute⁻¹. The tensile strains were gradually increased from 25% to 50%, 75%, 100%, and 250% without any resting time between cycles. To avoid significant plastic deformation beyond the yield stress, the maximum tensile strain was restricted to 250%, as this corresponds to the yield stress observed in most of the specimens. Energy dissipation within each hysteresis loop is calculated based on the area enclosed by the loop on the stress-strain curve.

Fourier transform infrared (FT-IR) spectroscopy was conducted using a Perkin Elmer Spectrum 2000 FTIR spectrometer (Waltham, United States) in transmission mode. The as-prepared hydrogel specimens were placed in a KBr pellet, and the spectra were recorded in the range of 1500 to 500 cm⁻¹ by accumulating 64 scans per spectrum with a resolution of 4 cm⁻¹.

Data availability

The authors declare that the main data supporting the findings of this study are available within the article and its Supplementary Information files. The data that support the findings of this study are openly available in Figshare at <https://doi.org/10.6084/m9.figshare.24022578.v1>. Additional data are available from the corresponding author upon request.

Received: 29 May 2023; Accepted: 11 September 2023;

Published online: 27 September 2023

References

1. Wu, Y. et al. Photocurable 3D printing of high toughness and self-healing hydrogels for customized wearable flexible sensors. *Adv. Funct. Mater.* **31**, 2107202 (2021).
2. Liu, R. et al. Highly tough, stretchable and resilient hydrogels strengthened with molecular springs and their application as a wearable, flexible sensor. *Chem. Eng. J.* **415**, 128839 (2021).
3. Hua, M. et al. Strong tough hydrogels via the synergy of freeze-casting and salting out. *Nature* **590**, 594–599 (2021).
4. Hua, M. et al. 4D printable tough and thermoresponsive hydrogels. *ACS Appl. Mater. Interf.* **13**, 12689–12697 (2021).
5. Lin, X., Zhao, X., Xu, C., Wang, L. & Xia, Y. Progress in the mechanical enhancement of hydrogels: Fabrication strategies and underlying mechanisms. *J. Poly. Sci.* **60**, 2525–2542 (2022).
6. Liu, C. et al. Tough hydrogels with rapid self-reinforcement. *Science* **372**, 1078–1081 (2021).
7. Guo, G. et al. 3D printing of tough hydrogels based on metal coordination with a two-step crosslinking strategy. *J. Mater. Chem. B* **10**, 2126–2134 (2022).
8. Chen, W. et al. Superstrong and tough hydrogel through physical cross-linking and molecular alignment. *Biomacromolecules* **20**, 4476–4484 (2019).
9. Lin, S. et al. Design of stiff, tough and stretchy hydrogel composites via nanoscale hybrid crosslinking and macroscale fiber reinforcement. *Soft Matter* **10**, 7519–7527 (2014).
10. Pruksawan, S. et al. Toughened hydrogels for 3D printing of soft auxetic structures. *Chem. – An Asian J.* **17**, e202200677 (2022).

11. Ahmed, E. M. Hydrogel: Preparation, characterization, and applications: A review. *J. Adv. Res.* **6**, 105–121 (2015).
12. Mohd Amin, M. C. I., Ahmad, N., Halib, N. & Ahmad, I. Synthesis and characterization of thermo- and pH-responsive bacterial cellulose/acrylic acid hydrogels for drug delivery. *Carbohydr. Polym.* **88**, 465–473 (2012).
13. Xu, W. et al. A stretchable solid-state zinc ion battery based on a cellulose nanofiber–polyacrylamide hydrogel electrolyte and a $\text{Mg}_{0.23}\text{V}_2\text{O}_5 \cdot 1.0\text{H}_2\text{O}$ cathode. *J. Mater. Chem. A* **8**, 18327–18337 (2020).
14. Kou, J. H., Amidon, G. L. & Lee, P. I. pH-dependent swelling and solute diffusion characteristics of poly(hydroxyethyl methacrylate–CO–methacrylic acid) hydrogels. *Pharmaceut. Res.* **5**, 592–597 (1988).
15. Fu, J. Strong and tough hydrogels crosslinked by multi-functional polymer colloids. *J. Poly. Sci. Part B: Polymer Phys.* **56**, 1336–1350 (2018).
16. Sun, Y., Liu, S., Du, G., Gao, G. & Fu, J. Multi-responsive and tough hydrogels based on triblock copolymer micelles as multi-functional macro-crosslinkers. *Chem. Commun.* **51**, 8512–8515 (2015).
17. Tan, M., Zhao, T., Huang, H. & Guo, M. Highly stretchable and resilient hydrogels from the copolymerization of acrylamide and a polymerizable macromolecular surfactant. *Poly. Chem.* **4**, 5570–5576 (2013).
18. Li, J. et al. Hofmeister effect mediated strong pHEMA-gelatin hydrogel actuator. *ACS Appl. Mater. Interf.* **14**, 23826–23838 (2022).
19. Furukawa, H., Horie, K., Nozaki, R. & Okada, M. Swelling-induced modulation of static and dynamic fluctuations in polyacrylamide gels observed by scanning microscopic light scattering. *Phys. Rev. E* **68**, 031406 (2003).
20. Costa, A. M. S. & Mano, J. F. Extremely strong and tough hydrogels as prospective candidates for tissue repair – A review. *European Poly. J.* **72**, 344–364 (2015).
21. Wang, M., Chi, H., K. S. J. & Wang, F. Progress in the synthesis of bifunctionalized polyhedral oligomeric silsesquioxane. *Polymers* **11**, 2098 (2019).
22. Wang, F., Lu, X. & He, C. Some recent developments of polyhedral oligomeric silsesquioxane (POSS)-based polymeric materials. *J. Mater. Chem.* **21**, 2775–2782 (2011).
23. Valiya Parambath, S., Ponnamma, D., Sadasivuni, K. K., Thomas, S. & Stephen, R. Effect of nanostructured polyhedral oligomeric silsesquioxane on the physical properties of poly(vinyl alcohol). *J. Appl. Poly. Sci.* **134**, 45447 (2017).
24. Divakaran, N. et al. Novel unsaturated polyester nanocomposites via hybrid 3D POSS-modified graphene oxide reinforcement: Electro-technical application perspective. *Nanomaterials* **10**, 260 (2020).
25. Thitsartarn, W. et al. Simultaneous enhancement of strength and toughness of epoxy using POSS-Rubber core-shell nanoparticles. *Comp. Sci. Technol.* **118**, 63–71 (2015).
26. Pruksawan, S. & Wang, F. Modeling of toughening effect in rigid particulate-filled polymer composites by artificial intelligence: a review. *Adv. Comp. Mater.* **32**, 250–267 (2023).
27. Blanco, I. The rediscovery of POSS: A molecule rather than a filler. *Polymers* **10**, 904 (2018).
28. Cohen, Y., Ramon, O., Kopelman, I. J. & Mizrahi, S. Characterization of inhomogeneous polyacrylamide hydrogels. *J. Poly. Sci. Part B: Poly. Phys.* **30**, 1055–1067 (1992).
29. Norioka, C., Inamoto, Y., Hajime, C., Kawamura, A. & Miyata, T. A universal method to easily design tough and stretchable hydrogels. *NPG Asia Mater.* **13**, 34 (2021).
30. Kishore, K. & Santhanalakshmi, K. N. Thermal polymerization of acrylamide by differential scanning calorimetry. *J. Poly. Sci.: Poly. Chem. Edit.* **19**, 2367–2375 (1981).
31. Rebers, L. et al. Differentiation of physical and chemical cross-linking in gelatin methacryloyl hydrogels. *Sci. Rep.* **11**, 3256 (2021).
32. Pawlak, A. The entanglements of macromolecules and their influence on the properties of polymers. *Macromol. Chem. Phys.* **220**, 1900043 (2019).
33. Yan, X. et al. High strength and self-healable gelatin/polyacrylamide double network hydrogels. *J. Mater. Chem. B* **5**, 7683–7691 (2017).
34. Gombert, Y., Roncoroni, F., S^vnchez-Ferrer, A. & Spencer, N. D. The hierarchical bulk molecular structure of poly(acrylamide) hydrogels: beyond the fishing net. *Soft Matter* **16**, 9789–9798 (2020).
35. Fan, J., Shi, Z., Lian, M., Li, H. & Yin, J. Mechanically strong graphene oxide/sodium alginate/polyacrylamide nanocomposite hydrogel with improved dye adsorption capacity. *J. Mater. Chem. A* **1**, 7433–7443 (2013).
36. Zhou, C. & Wu, Q. A novel polyacrylamide nanocomposite hydrogel reinforced with natural chitosan nanofibers. *Coll. Surf. B: Biointerf.* **84**, 155–162 (2011).
37. Turner, D. T. Glass transition elevation by polymer entanglements. *Polymer* **19**, 789–796 (1978).
38. Chen, H. et al. A comparative study of the mechanical properties of hybrid double-network hydrogels in swollen and as-prepared states. *J. Mater. Chem. B* **4**, 5814–5824 (2016).
39. Dmitriev, I., Kuryndin, I., Bobrova, N. & Smirnov, M. Swelling behavior and network characterization of hydrogels from linear polyacrylamide crosslinked with glutaraldehyde. *Mater. Today Commun.* **4**, 93–100 (2015).
40. Bahrami, Z., Akbari, A. & Eftekhari-Sis, B. Double network hydrogel of sodium alginate/polyacrylamide cross-linked with POSS: Swelling, dye removal and mechanical properties. *Int. J. Biol. Macromol.* **129**, 187–197 (2019).
41. Prządka, D., Andrzejewska, E. & Marcinkowska, A. Multimethacryloxy-POSS as a crosslinker for hydrogel materials. *Eur. Poly. J.* **72**, 34–49 (2015).
42. Eshel, H., Dahan, L., Dotan, A., Dodiuk, H. & Kenig, S. Nanotailoring of nanocomposite hydrogels containing POSS. *Poly. Bull.* **61**, 257–265 (2008).
43. Wang, J., Sutti, A., Wang, X. & Lin, T. Fast responsive and morphologically robust thermo-responsive hydrogel nanofibres from poly(N-isopropylacrylamide) and POSS crosslinker. *Soft Matter* **7**, 4364–4369 (2011).
44. Zhang, X. et al. Enhanced mechanical properties and self-healing behavior of PNIPAM nanocomposite hydrogel by using POSS as a physical crosslinker. *J. Appl. Poly. Sci.* **137**, 48486 (2020).
45. Sabbagh, F. & Muhamad, I. I. Acrylamide-based hydrogel drug delivery systems: Release of Acyclovir from MgO nanocomposite hydrogel. *J. Taiwan Instit. Chem. Eng.* **72**, 182–193 (2017).
46. Zheng, H. et al. UV-initiated polymerization of cationic polyacrylamide: Synthesis, characterization, and sludge dewatering performance. *Sci. World J* **2013**, 937937 (2013).
47. Gong, J. P., Katsuyama, Y., Kurokawa, T. & Osada, Y. Double-network hydrogels with extremely high mechanical strength. *Adv. Mater.* **15**, 1155–1158 (2003).
48. Ito, K. Novel cross-linking concept of polymer network: Synthesis, structure, and properties of slide-ring gels with freely movable junctions. *Polymer J.* **39**, 489–499 (2007).
49. Haraguchi, K. & Takehisa, T. Nanocomposite hydrogels: A unique organic–inorganic network structure with extraordinary mechanical, optical, and swelling/de-swelling properties. *Adv. Mater.* **14**, 1120–1124 (2002).
50. Hu, Z. & Chen, G. Novel nanocomposite hydrogels consisting of layered double hydroxide with ultrahigh tensibility and hierarchical porous structure at low inorganic content. *Adv. Mater.* **26**, 5950–5956 (2014).
51. Chen, F. et al. Fabrication and mechanical behaviors of novel supramolecular/polymer hybrid double network hydrogels. *Polymer* **168**, 159–167 (2019).
52. Li, S.-N. et al. Mechanically robust polyacrylamide composite hydrogel achieved by Integrating lamellar montmorillonite and chitosan microcrystalline structure into covalently cross-linked network. *ACS Appl. Poly. Mater.* **2**, 1874–1885 (2020).
53. Liu, R. et al. Tough and highly stretchable graphene oxide/polyacrylamide nanocomposite hydrogels. *J. Mater. Chem.* **22**, 14160–14167 (2012).
54. Yang, C. H. et al. Strengthening alginate/polyacrylamide hydrogels using various multivalent cations. *ACS Appl. Mater. Interf.* **5**, 10418–10422 (2013).
55. Sujian, M. I. et al. Bi-functional silica nanoparticles for simultaneous enhancement of mechanical strength and swelling capacity of hydrogels. *RSC Adv.* **10**, 6213–6222 (2020).
56. Yang, J. et al. Synthetic and viscoelastic behaviors of silica nanoparticle reinforced poly(acrylamide) core-shell nanocomposite hydrogels. *Soft Matter* **9**, 1220–1230 (2013).
57. Mo, K., Zhang, T., Yan, W. & Chang, C. Tunicate cellulose nanocrystal reinforced polyacrylamide hydrogels with tunable mechanical performance. *Cellulose* **25**, 6561–6570 (2018).
58. Dorishetty, P., Dutta, N. K. & Choudhury, N. R. Bioprintable tough hydrogels for tissue engineering applications. *Adv. Coll. Interf. Sci.* **281**, 102163 (2020).
59. Liu, Y., He, W., Zhang, Z. & Lee, B. P. Recent developments in tough hydrogels for biomedical applications. *Gels* **4**, 46 (2018).
60. Ferreira, L. M. et al. Polyacrylamide hydrogel containing calendula extract as a wound healing bandage: In vivo test. *Int. J. Mol. Sci.* **24**, 3806 (2023).
61. Polu, A. R. et al. Effect of POSS-PEG hybrid nanoparticles on cycling performance of polyether-LiDFOB based solid polymer electrolytes for all solid-state Li-ion battery applications. *J. Indust. Eng. Chem.* **45**, 68–77 (2017).
62. Chinnam, P. R., Zhang, H. & Wunder, S. L. Blends of pegylated polyoctahedralsilsesquioxanes (POSS-PEG) and methyl cellulose as solid polymer electrolytes for lithium batteries. *Electrochim. Acta* **170**, 191–201 (2015).
63. Pruksawan, S. et al. Gold nanorods function as near-infrared light-activated microheaters for in situ curing of injectable hydrogel therapies. *ACS Appl. Poly. Mater.* **5**, 4565–4577 (2023).

Acknowledgements

This work was financially supported by SERC Central Research Fund (SC25/21-110915) of Agency for Science, Technology and Research (A*STAR) of Singapore and the Bio-medical Engineering Programme (BEP) (C221318002).

Author contributions

S.P. and F.W. conceived the idea, developed the outline, designed the experiment; J.W.R.L. synthesized and characterized the POSS-PEG; S.P., Y.L.L., Z.L. prepared samples and performed the experimental measurements; S.P., Y.L.L. and Y.T.C. carried out the photo-DSC measurements with the help of H.L.C; S.P., H.C. and F.W. analyzed the data and wrote the manuscript with contributions from all authors.

Competing interests

The authors declare no competing interests.

Additional information

Supplementary information The online version contains supplementary material available at <https://doi.org/10.1038/s43246-023-00402-2>.

Correspondence and requests for materials should be addressed to Hong Chi or FuKe Wang.

Peer review information *Communications Materials* thanks the anonymous reviewers for their contribution to the peer review of this work. Primary Handling Editor: Jet-Sing Lee. A peer review file is available

Reprints and permission information is available at <http://www.nature.com/reprints>

Publisher's note Springer Nature remains neutral with regard to jurisdictional claims in published maps and institutional affiliations.



Open Access This article is licensed under a Creative Commons Attribution 4.0 International License, which permits use, sharing, adaptation, distribution and reproduction in any medium or format, as long as you give appropriate credit to the original author(s) and the source, provide a link to the Creative Commons licence, and indicate if changes were made. The images or other third party material in this article are included in the article's Creative Commons licence, unless indicated otherwise in a credit line to the material. If material is not included in the article's Creative Commons licence and your intended use is not permitted by statutory regulation or exceeds the permitted use, you will need to obtain permission directly from the copyright holder. To view a copy of this licence, visit <http://creativecommons.org/licenses/by/4.0/>.

© The Author(s) 2023